Available online at www.sciencedirect.com
SCIENCE DIRECT®
Acta Materialia 52 (2004) 3793–3805
Acta MATERIALIA
www.actamat-journals.com

Transformations of grain boundaries in deformed nanocrystalline materials

S.V. Bobylev, M. Yu. Gutkin *, I.A. Ovid'ko

Institute of Problems of Mechanical Engineering, Russian Academy of Sciences, Bolshoj 61, Vas. Ostrov, St. Petersburg 199178, Russia

Received 16 March 2004; received in revised form 26 April 2004; accepted 28 April 2004
Available online 10 June 2004

Abstract

Theoretical models are suggested which describe transformations of grain boundaries in nanocrystalline materials under plastic deformation. We consider such transformations as decay of low-angle grain boundaries, bowing of high-angle grain boundaries, and emission of partial dislocations by grain boundaries in deformed nanocrystalline materials. In the framework of the suggested model description, lattice dislocations that form a low-angle tilt boundary glide under the action of the forces owing to external (applied) and internal stresses. The balance of the forces causes the critical shear stress at which the low-angle boundary decays. Such decay processes result in the formation of high-density ensembles of mobile lattice dislocations that are capable of inducing plastic flow localization (shear banding) in mechanically loaded nanocrystalline materials. High-angle grain boundaries are modeled as those containing grain boundary dislocations with small Burgers vectors. The movement of grain boundary dislocations under the shear stress action gives rise to bowing of high-angle boundaries. In certain ranges of parameters, grain boundary dislocations undergo splitting transformations followed by emission of partial dislocations from high-angle boundaries into adjacent grain interiors. The models account for experimental data reported in the literature.

Keywords: Deformation; Grain boundaries; Dislocations; Nanostructures

1. Introduction

Transformations of grain boundaries (GBs) often strongly influence both the structure and the properties of nanocrystalline and polycrystalline materials, e.g., [1–29]. Thus, plastic deformation processes in nanocrystalline materials (NCMs) are associated with transformations of GBs and GB defect ensembles, that crucially affect the structure and outstanding mechanical characteristics of such materials; see, e.g., experimental data [1–10], theoretical models [11–20] and molecular dynamics simulations [21–25]. Among the most important issues for the mechanical behavior (in particular, ductility and superplasticity) of NCMs is their ability to suppress plastic flow localization in shear bands, nuclei of the necking [2,30,31]. This has generated interest in the identification of the role of GBs and their transformations in the formation and evolution of shear bands in NCMs, which potentially will allow one to influence the processes of plastic flow localization. In particular, in ductile NCMs with comparatively large grains with size $d \geqslant 30$ nm, where the lattice dislocation slip is dominant, GBs can serve as effective sources of perfect lattice dislocations and partial lattice dislocations providing deformation twinning [1,32–35]. (Molecular dynamics simulations [21–24] have predicted deformation twinning. However, this approach allows one to predict the deformation mode, but not to describe its characteristics.)

In previous theoretical models [15,36,37] of emission of perfect lattice dislocations by high-angle GBs in nano- and fine-grained materials, intensity of the emission events was assumed to be controlled by movement and transformations of GB dislocations and disclinations. These processes are too slow to cause the formation of high-density ensembles of mobile lattice

* Corresponding author. Tel.: +7-812-3214764; fax: +7-812-3214771.
E-mail addresses: gutkin@def.ipme.ru (M.Y. Gutkin), ovidko@def.ipme.ru (I.A. Ovid'ko).

1359-6454/$30.00 © 2004 Acta Materialia Inc. Published by Elsevier Ltd. All rights reserved.
doi:10.1016/j.actamat.2004.04.029

dislocations that would carry large plastic strains in shear bands. At the same time, NCMs contain low-angle boundaries consisting of lattice dislocations [38]. Such low-angle boundaries undergo structural transformations under the action of internal stresses in coarse-grained polycrystalline materials (see [26–29] and references therein), in which case it is natural to think that low-angle boundaries can undergo dramatic transformations under the action of applied stresses in mechanically loaded NCMs, too.

The main aim of this paper is to describe in detail the decays of low-angle tilt boundaries (briefly discussed earlier in [18]) under the shear stress action as processes that produce high-density ensembles of mobile lattice dislocations in local regions of NCMs (see Sections 2–4). Also, a theoretical model (see Section 5) is suggested to investigate very similar transformations of high-angle GBs, which are bowing of GBs and emission of partial dislocations (associated with deformation twinning) from high-angle GBs under the shear stress action. These models account for experimental observations [1,32–35] of the transformations of GB structures, which are capable of playing an essential role in the deformation behavior of NCMs.

2. Decay of low-angle tilt boundaries in nanocrystalline materials: model

Consider a model low-angle tilt boundary terminated at triple junctions of GBs in a nanocrystalline sample (Fig. 1(a)). The low-angle boundary in its initial state (in the absence of mechanical load) is represented as a straight wall of periodically arranged edge dislocations with Burgers vector $\boldsymbol{b}$. The low-angle boundary is characterized by the tilt misorientation angle θ being in the Frank relationship, $\sin(\theta/2) = b/(2h)$ [25], with parameters (the period h and the Burgers vector magnitude b) of the dislocation arrangement in the boundary. Also, for definiteness, the tilt misorientation θ is assumed to be in compensating relationships, $\theta + \theta_1 + \theta_2 = 0$ and $-\theta + \theta'_1 + \theta'_2 = 0$, with the tilt misorientation parameters, (θ_1, θ_2) and (θ'_1, θ'_2), of the GBs adjacent to the upper and bottom triple junctions, respectively, shown in Fig. 1(a). In other words, the finite dislocation wall in its initial state (Fig. 1(a)) is terminated by disclinations that completely compensate for the disclination defects (shown as triangles in Fig. 1) at the upper and bottom junctions of its adjacent GBs characterized by the tilt misorientation parameters, (θ_1, θ_2) and (θ'_1, θ'_2), respectively.

The action of a shear stress τ on the edge dislocations composing the low-angle tilt boundary in a mechanically loaded nanocrystalline sample causes displacements of these dislocations (Fig. 1(b)) from their initial positions shown in Fig. 1(a). In other words, the shear stress action causes bowing of the low-angle tilt boundary. At some critical value τ_c of the shear stress, one of the edge lattice dislocations composing the low-angle boundary releases and starts moving far from the initial boundary plane (Fig. 1(c)). As is evident (and proved by further analysis in this paper), the release of the first dislocation from the low-angle boundary (Fig. 1(c)) is immediately followed by decay of the boundary (dislocation wall) as a whole (Fig. 1(d)). As a result, a group of lattice dislocations released from the decayed low-angle boundary move, causing local plastic deformation and the formation of an elongated grain. Following experimental data [2,39], such elongated grains are characteristic structural elements of shear bands in nanocrystalline Fe.

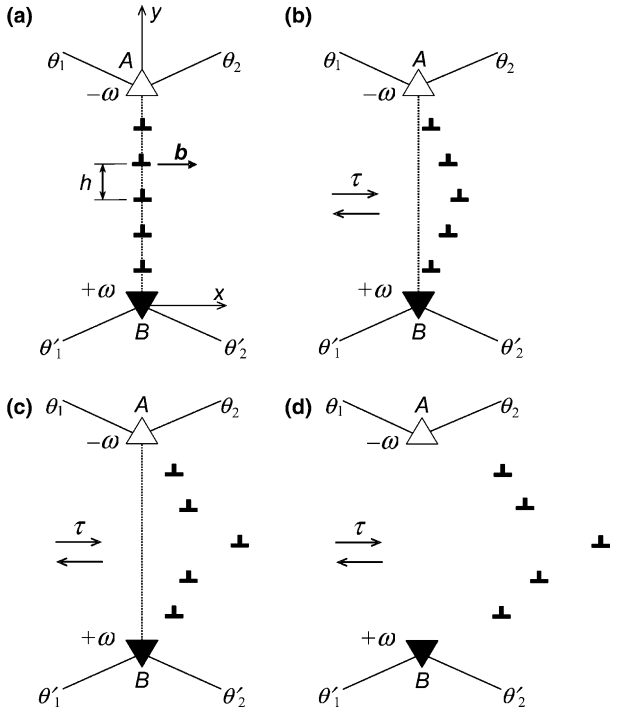

Fig. 1. Decay of a low-angle tilt boundary represented as a periodic dislocation wall terminated at triple junctions A and B. (a) Dislocation wall in its initial state (in the absence of mechanical load). (b) Shear stress τ causes bowing of the dislocation wall. (c) One of the dislocations releases from the dislocation wall. (d) Dislocation wall completely decays resulting in formation of a dipole of uncompensated disclinations with the strengths $-\omega$ and $+\omega$ at triple junctions A and B, respectively.

Notice that the decay of the low-angle boundary removes it from the triple junctions which thereby transform into uncompensated double junctions (Fig. 1(d)). The upper and lower junctions become uncompensated stress sources of the disclination type, characterized by disclination strength $-\omega = -\theta$ and $\omega = \theta$, respectively. The stress field of the disclination dipole serves as the hampering force for movement (release) of the lattice dislocations from the low-angle tilt boundary and its decay. It is taken into account in our calculations of the critical shear stress τ_c (at which the decay occurs) in the

next section. Also, notice that there is an increase in the rms internal stresses when low-angle boundaries break and the stress fields of diclination dipoles come into play. This increase may be detected in experiments.

3. Critical shear stress for decay of low-angle tilt boundaries in deformed nanocrystalline materials

Let us calculate the critical shear stress τ_c by methods of two-dimensional dislocation dynamics. The two-dimensional approach allows us to catch the principal peculiarities of the decay process and estimate the τ_c in the first approximation. At the same time, the two-dimensional approach can serve as an effective basis for further investigations with using methods of the three-dimensional dislocation dynamics.

Each dislocation in the low-angle boundary in a mechanically loaded NCM (Fig. 1(b)) is under combined action of the forces caused by the shear stress, other dislocations belonging to the boundary, and the disclination dipole. Let us calculate these forces and write the corresponding equations for dislocation movement. In doing so, we assume that dislocations can move along one slip plane (along x-axis in the coordinate system shown in Fig. 1(a)), in which case the only x-projections of the forces play the role. Solution of the system of equations, describing one-dimensional movement of dislocations, will be expressed as dependences $x_i(t)$, where x_i is the coordinate of the ith dislocation ($i = 1, 2, \ldots, N$), and t is time.

In the framework of the approach discussed, the force acting on the ith dislocation belonging to the low-angle boundary may be written as follows:

$$F_i = b\left[\tau + Db\sum_{\substack{k=1\\k\neq i}}^{N}\frac{(x_i-x_k)\{(x_i-x_k)^2-(y_i-y_k)^2\}}{\{(x_i-x_k)^2+(y_i-y_k)^2\}^2} - D\omega\left(\frac{x_i y_i}{x_i^2+y_i^2}-\frac{x_i(y_i-d)}{x_i^2+(y_i-d)^2}\right)\right], \quad (1)$$

where $D = G/[2\pi(1-\nu)]$, G is the shear modulus, ν is the Poisson ratio, x_i and $y_i = ih$ are the coordinates of the ith dislocation, and d denotes the tilt boundary length (the distance between the triple junction disclinations that form the dipole; see Fig. 1). The first term of formula (1) describes the force due to the shear stress τ, the second one the force of interaction with the other dislocations of the boundary [40], and the third one the force of interaction with the disclination dipole [41].

With the forces given by formula (1), equations for movement of the dislocations composing the low-angle tilt boundary (Fig. 1(a)) read

$$m\frac{d^2x_i}{dt^2}+\beta\frac{dx_i}{dt}=F_i, \quad i=1,2,\ldots,N. \quad (2)$$

First derivatives dx_i/dt in these equations take into account the dislocation movement friction (associated with the dynamic retardation of the crystalline lattice to dislocation movement), and β is the viscosity coefficient. The dislocation mass m is given by the standard approximation [42], $m = \rho b^2/2$, where ρ is the material density.

To solve numerically the system of equations (2), we have used the conventional software Mathematica 4. The following characteristic values of parameters have been chosen for the exemplary case of nanocrystalline Fe (whose deformation behavior had been experimentally studied in papers [2,39]): $G = 82$ GPa, $\nu = 0.29$, lattice parameter $a = 0.287$ nm, $b = \frac{1}{2}a\langle 1\,1\,1\rangle = 0.25$ nm, $\rho = 7800$ kg m^{-3}, dislocation mass (per unit length of dislocation line) $m = 2.4\times10^{-16}$ kg m^{-1}, and $\beta \approx 5\times10^{-5}$ Pa s [42]. For these values of parameters, we have considered the behavior of a low-angle tilt boundary composed of $N = 15$ dislocations and characterized by tilt misorientation angle $\theta = 0.1$ ($\approx 5.7°$), in which case $\omega = 0.1$ and $h = 10b$.

Some typical plots $x(t)$ (for the 8th, the central dislocation), have been calculated at different values of τ ranged from 0.5 to 1.54 GPa (see Fig. 2). For relatively low stress values (here <1.53 GPa), the dislocation makes some oscillations and is finally stabilized at some equilibrium position which is shifted further with the increasing stress value (curves 1–4 in Fig. 2). When the stress magnitude becomes larger than a critical value τ_c (here $\tau_c = 1.53$ GPa), the dislocation moves far away from its initial position (curve 6 in Fig. 2).

Since our model deals with only low-angle boundaries, the maximum possible misorientation angle is about 10°, in which case $h \approx 5.7b$. The low-angle boundary should contain at least three ($N_{min} = 3$) dislocations. In these circumstances, minimum bound-

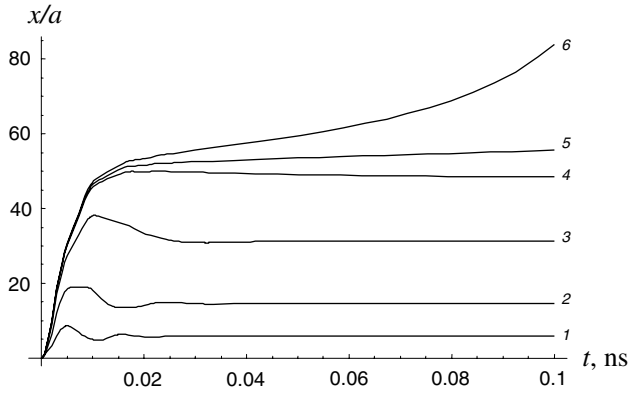

Fig. 2. Dependences of coordinate x on time t for the 8th dislocation in a low-angle boundary characterized by the misorientation $\theta = 0.1$ and composed of $N = 15$ dislocations, for the shear stress $\tau = 0.5$, 1.0, 1.4, 1.52, 1.53 and 1.54 GPa (curves 1, 2, 3, 4, 5 and 6, respectively).

ary length (grain size), below which our model is inapplicable, equals $d_{\min} = (N_{\min} + 1)h \approx 22.8b$. In the exemplary case of nanocrystalline Fe this gives $d_{\min} \approx 5.7$ nm.

As noted earlier, the decay of the boundary begins at its centre when the 8th (central) dislocation is released from the boundary (Fig. 1(c)). Following our calculations, immediately after the central dislocation has moved far enough from the initial boundary plane (Fig. 1(c)), the boundary dramatically decays as a whole (Fig. 1(d)). That is, all the dislocations composing the boundary move far from its plane during a very short time interval. In these circumstances, in order to calculate critical parameters at which the low-angle boundary decays as a whole, it is sufficient to characterize the behavior of only one (central) dislocation.

In this manner, we have analyzed stability and decay of low-angle tilt boundaries with different parameters. This has allowed us to reveal critical values of the shear stress τ_c at which the decay (Fig. 1) of low-angle tilt boundaries with different characteristics occurs. The dependence of τ_c on boundary misorientation θ is shown in Fig. 3, for $N = 5$, 15, and 30. As follows from Fig. 3, τ grows in a tentatively linear way with rising θ. It is indicative of the crucial contribution of the boundary misorientation and thereby the strength of the disclination dipole to the stability of low-angle tilt boundaries under the shear stress action. Curves corresponding to different values of parameter N at a constant value of θ are very close. This means that the dependence of τ_c on the number N of dislocations and thereby the boundary length $d(= Nh)$ at a constant value of θ is very weak. In this context, in particular, very short GBs in very small grains and comparatively long GBs in large grains decays at close values of the critical stress τ_c, if they have the same misorientation parameters. At the same time, the action of Frank–Read sources of lattice dislocations is suppressed in very small grains of NCMs [43] in which

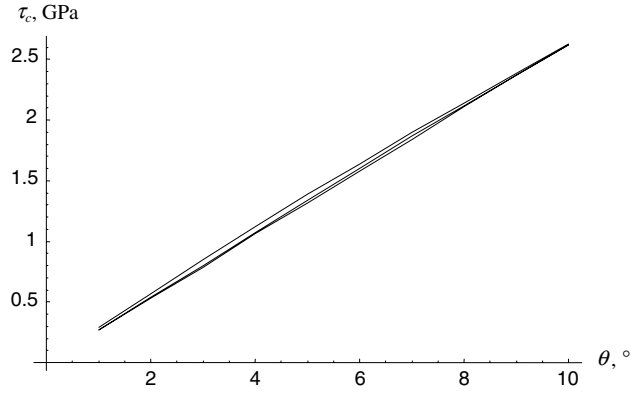

Fig. 3. Dependence of the critical shear stress τ_c on the misorientation angle θ of a tilt boundary consisting of $N = 5$, 15 and 30 edge dislocations (from top to bottom).

only the decay of low-angle boundaries provides the effective generation of mobile lattice dislocations. In this event, τ_c represents a very important characteristic of plastic flow in NCMs. In contrast, in conventional coarse-grained polycrystalline materials, where Frank–Read sources are activated at shear stresses lower than τ_c, the decay of low-angle boundaries does not play any essential role in plastic deformation processes.

The decay of a low-angle tilt boundary in a mechanically loaded nanocrystalline sample results in the formation of moving lattice dislocations that carry local plastic deformation and come to the neighbouring GBs (Fig. 1(d)). The moving lattice dislocations elastically interact with other lattice dislocations composing neighbouring low-angle GBs. This interaction is able of causing decays of the neighbouring low-angle GBs, accompanied by avalanche-like release of new mobile lattice dislocations.

For illustration, let us briefly discuss the effects of the lattice dislocations that are released from the decay of the low-angle tilt boundary AB and move towards its neighboring low-angle tilt boundary KL (Fig. 4). In doing so, we distinguish the two cases. In the first case (Fig. 4(a)), the moving dislocations released from the decay of the boundary AB and immobile dislocations composing the boundary KL have Burgers vectors with opposite signs. The system in its initial state contains the low-angle tilt boundary KL which is curved due to the shear stress action. The lattice dislocations, released from the decay of the neighboring low-angle tilt boundary AB and shown by the open dislocation signs, move towards the boundary KL which consists of the lattice dislocations shown by the solid dislocation signs. The moving dislocations are elastically attracted by the immobile dislocations and some of them annihilate. The annihilation reduces the tilt misorientation of the boundary KL which thereby becomes able of decaying at the given level of the shear stress. (We consider the only case of $\omega_l < \omega$, because, in the opposite case, the critical shear stress for decay of the boundary KL with misorientation $\omega < \omega_l$ is lower than that for decay of the boundary AB. That is, in the case of $\omega < \omega_l$, the boundary KL would decay before the boundary AB.)

Fig. 4(b) illustrates the situation where the mobile dislocations (released from decay of the low-angle tilt boundary AB) have the same Burgers vector sign as the immobile dislocations composing the low-angle tilt boundary KL. The mobile dislocations elastically interact with the immobile dislocations, providing the shear stress concentration. In this case the effective value of the shear stress acting on the immobile dislocations of the boundary KL is larger than applied shear stress. This effective shear stress is able of causing the decay of the boundary KL.

To summarize, in the situations illustrated in Fig. 4, the decay of a low-angle tilt boundary AB, followed by a

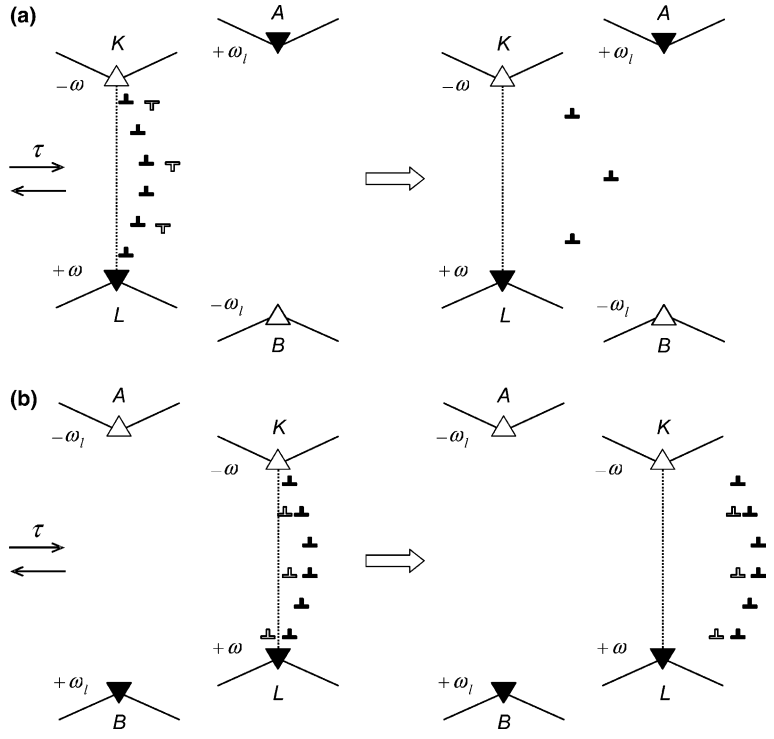

Fig. 4. Movement of lattice dislocations (open dislocation signs) released from decay of low-angle tilt boundary AB towards neighboring boundary KL in the cases where moving and immobile dislocations have Burgers vectors of (a) the opposite signs and (b) the same sign.

release of lattice dislocations, enhances the decay of the neighboring low-angle tilt boundary KL. This effect occurs due to the interaction between the mobile dislocations released from decay of the low-angle tilt boundary AB and the immobile dislocations composing the low-angle tilt boundary KL.

4. Low-angle boundary in the stress field of decayed neighbouring boundary

After a low-angle tilt boundary has decayed, it has become a stress source of the disclination dipole type. More precisely, two wedge disclinations of opposite strength $\pm\omega_l$ are formed at the grain boundary junctions after the low-angle boundary dislocations have moved far from the initial boundary plane (Fig. 5). This disclination dipole elastically interacts with defects located in its vicinity. In particular, the disclination dipole either attracts or repels lattice dislocations composing neighboring grain boundaries, depending on geometry of the defect system. This elastic interaction plays the role of the key factor initiating decay of the neighboring boundary KL, if the mobile dislocations released from decay of the low-angle tilt boundary AB move in the direction opposite to this boundary (Fig. 5). The two basic variants of geometry of the two boundaries AB and KL in the situation under consideration are shown in Fig. 5. The boundary junction disclinations A and B (resulted from decay of a low-angle tilt boundary) are characterized by the disclination strength values $\pm\omega_l$ and distant by d_l from each other. The neighboring low-angle tilt boundary KL is characterized by the misorientation ω and the length d. The distance between the decayed AB and neighbouring KL boundary planes is l. The tilt misorientation ω of the boundary KL is in the corresponding compensating relationships with the tilt misorientation parameters of the GBs adjacent to the bottom and upper triple junctions K and L (Fig. 5), respectively. In other words, the finite dislocation wall—the neighbouring tilt boundary—in its initial state is terminated by two wedge disclinations that completely compensate for the disclination defects (shown as triangles in Fig. 5) at the junctions K and L of its adjacent GBs.

There is a situation (Fig. 5(a)) where the disclination dipoles AB and KL have the same sign (the disclinations located at the upper junctions A and K are both negative or, in equivalent terms, the disclinations located at the bottom junctions B and L are both positive). In this case, the stress field of the disclination dipole AB attracts the dislocations, composing the grain boundary KL, thus causing an enhancement of the decay of the neighbouring low-angle tilt boundary KL.

The opposite situation (Fig. 5(b)) is realized when the disclination dipoles AB and KL have opposite signs, that is, the disclinations located at the upper junctions A and K have strength values of opposite signs. (The same

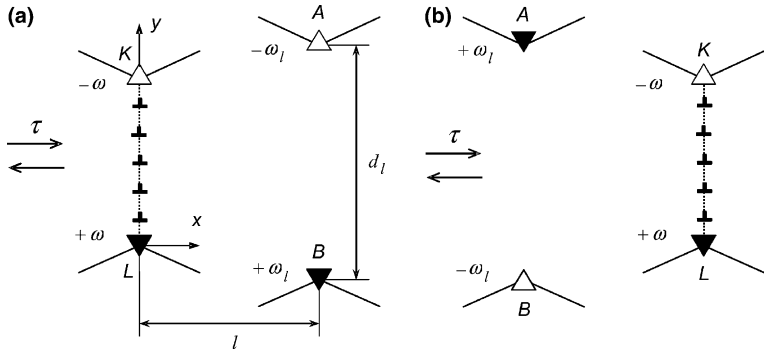

Fig. 5. Two low-angle boundaries, boundary KL and decayed boundary AB, under the shear stress action. The disclinations (open and full triangles) at boundary junctions A and B create the stress fields whose superposition enhances decay of low-angle boundary KL. Two variants of geometry of boundaries are shown in (a) and (b).

is true for the disclinations located at the bottom junctions B and L; see Fig. 5(b).) In this case, the stress field of the disclination dipole AB repels the dislocations, composing the grain boundary KL, but here the decayed boundary AB is located on the other side of the boundary KL (compared to the previous configuration in Fig. 5(a)). Therefore, the stress field of the disclination dipole AB causes an enhancement of the decay of the neighbouring low-angle tilt boundary KL in this case as well.

Thus, we can conclude that generally the decay of one low-angle tilt boundary (AB) leads to softening of the material in a local area in its vicinity.

In this paper, we will analyse in detail the exemplary case shown in Fig. 5(a). In the case discussed, in order to describe the behavior of lattice dislocations composing the neighbouring boundary KL, we will use the same calculation scheme as with the previously considered decay of the low-angle tilt boundary AB (see Section 3). The difference between these cases is in the expression for the force F_i acting on the ith dislocation in a tilt boundary. More precisely, in the case of the boundary KL (Fig. 5(a)), the force F_i is given by formula (1) where the stress field of the disclination dipole AB is added. In doing so, we have the following expression for the force:

$$F_i = b\left[\tau + Db\sum_{\substack{k=1\\k\neq i}}^{N}\frac{(x_i-x_k)\{(x_i-x_k)^2-(y_i-y_k)^2\}}{\{(x_i-x_k)^2+(y_i-y_k)^2\}^2} - D\omega\left(\frac{x_iy_i}{x_i^2+y_i^2}-\frac{x_i(y_i-d)}{x_i^2+(y_i-d)^2}\right) - D\omega_l\left(\frac{(x_i-l)(y_i+d_l/2-d/2)}{(x_i-l)^2+(y_i+d_l/2-d/2)^2} - \frac{(x_i-l)(y_i-d_l/2-d/2)}{(x_i-l)^2+(y_i-d_l/2-d/2)^2}\right)\right]. \quad (3)$$

For the same values of parameters as with the previous section, we have solved the system (2) with the right-hand side given by formula (3), for various values of ω_l, d_l and l. The results are presented in Fig. 6 for the case where $d_l = d$ and the disclination dipole is distant by $l = 50$ nm from the low-angle tilt boundary KL. The upper curve 1 in Fig. 6 corresponds to the dependence $\tau_c(\theta)$ in the situation when the disclination dipole is absent ($\omega_l = 0$). Curves 2, 3 and 4 in Fig. 6 show the dependences $\tau_c(\theta)$ for $\omega_l = 1°$, 3° and 5°, respectively. These curves are calculated in the range of $\omega_l \leqslant \theta \leqslant 10°$. The case of $\theta < \omega_l$ is not considered, because the critical shear stress for decay of the boundary KL with misorientation $\theta < \omega_l$ is lower than that for decay of the boundary AB. As was expected, the critical shear stress τ_c decreases with rising ω_l. This decrease is essential at certain values of parameters θ and ω_l, as illustrated in Fig. 6. For instance, for $\theta = 8.5°$, the critical stress τ_c at $\omega_l = 5°$ is lower by about 40% than that at $\omega_l = 0°$.

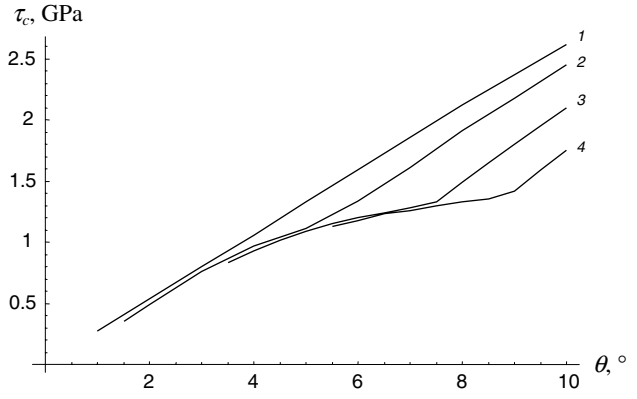

Fig. 6. Dependences of the critical shear stress τ_c (for decay of low-angle tilt boundary KL in the stress field of decayed boundary AB) on the misorientation angle θ of tilt boundary KL, for the disclination strength values of $\omega_l = 0°$, 1°, 3°, and 5° (curves 1, 2, 3, and 4, respectively).

It should be noted that the lattice dislocations released from decay of a low-angle tilt boundary KL in the stress field of the disclination dipole AB (Fig. 5(a)) can be stopped at the neighboring decayed boundary AB plane. The dislocations reach the boundary AB plane where they become immobile due to the elastic interaction with the disclination dipole AB. In other words, the dislocations transfer from one low-angle tilt boundary KL to another (previously decayed) boundary AB. Our calculations show that this phenomenon comes into play when misorientation values characterizing the boundaries KL and AB are close ($\omega \approx \omega_l$) and/or the boundaries are closely distant from each other ($l \approx d$).

To summarize, the stress field of a decayed low-angle tilt boundary, modeled as the stress field of the disclination dipole (Fig. 5), strongly influences the decay of its neighbouring low-angle boundary. In some cases, this influence significantly enhances the decay of a low-angle tilt boundary. The phenomenon in question is able of causing plastic flow localization (carried by lattice dislocations released by low-angle tilt boundaries) in deformed NCMs containing high-density ensembles of low-angle GBs.

5. Evolution of high-angle grain boundaries under the shear stress action in deformed nanocrystalline materials

Consider now the behavior of high-angle GBs in deformed NCMs. As shown experimentally, high-angle boundaries bow (become curved) [1,33] and emit partial lattice dislocations [32–35] that can provide deformation twinning in mechanically loaded NCMs. To account for these experimental data, here we will extend our theoretical model of the stress-induced evolution of low-angle tilt boundaries (see Sections 2–4) to the case of high-angle GBs containing GB dislocations.

In general, high-angle GBs contain intrinsic dislocations associated with misorientation mismatch at such boundaries and characterized by small Burgers vectors being lattice vectors of displacement-shift-complete lattices characterizing translational symmetries of GBs; see, e.g., [25]. (In short, a displacement-shift-complete lattice of a GB is formed by relative displacements of two crystals adjacent to the boundary, which conserve GB symmetry; for details, see [25].) Such dislocations in high-angle GBs cannot glide easily in the grain interior, in contrast to lattice dislocations composing low-angle tilt boundaries. Therefore, the decay of high-angle GBs under the shear stress action is not possible. At the same time, following experimental data [1,32–35], high-angle GBs bow (become curved) and emit partial dislocations into adjacent grain interiors in mechanically loaded NCMs. In this section, we elaborate a theoretical description of bowing and dislocation emission (Fig. 7),

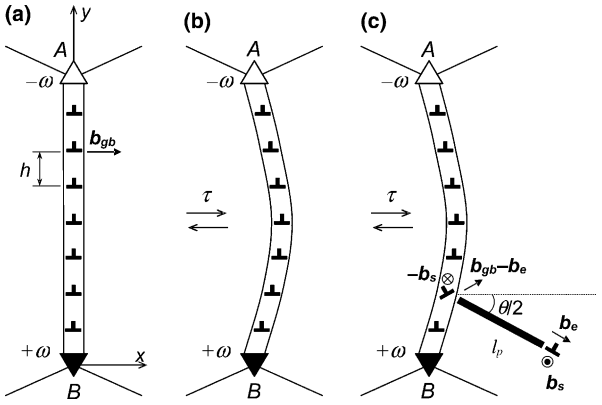

Fig. 7. Evolution of high-angle boundary with dislocations. (a) Initial state. (b) Bowing of boundary under the shear stress τ action. (c) Shear-stress-induced splitting of a grain boundary dislocation results in both the formation of an immobile grain boundary dislocation and emission of a partial Shockley dislocation into the grain interior. A stacking fault is formed behind the moving Shockley dislocation.

using the approach developed in the previous sections to analyze the behavior of low-angle tilt boundaries.

In the framework of our model, first we will describe the GB bowing, that is, transformation of a high-angle GB from its initial straight state (Fig. 7(a)) into the curved state (Fig. 7(b)) under the shear stress action. In doing so, we will use dislocation dynamics equations (2), as with a low-angle tilt boundary. The movement of a high-angle GB, resulting in its curvature, is a kind of shear-stress-induced GB migration accompanied by an increase of the GB length. The increase in the GB length leads to an increase of the GB energy by amount of ΔW_{gb}, which causes the hampering force F^{gb} for the GB bowing. This is taken into account in formula (5) describing the force acting on GB dislocations in a high-angle GB under the shear stress action.

Notice that intrinsic GB dislocations in high-angle GBs are defined [25] as dislocations associated with deviation of the boundary tilt misorientation from that of a low-energy (favorable) GB in the same material. In the context of this definition, the boundary tilt misorientation θ is in the following relationship (different from the standard Frank formula) with the parameters of the GB dislocation structure [25]:

$$2\sin\left(\frac{\theta-\theta_0}{2}\right) = b_{\mathrm{gb}}/h. \tag{4}$$

Here b_{gb} denotes the Burgers vector magnitude for a GB dislocation, and θ_0 is the tilt misorientation of the low-energy (favorable) boundary treated to be dislocation-free. Formula (4) looks like the Frank formula, in which the boundary misorientation θ is replaced by a difference $\theta-\theta_0$ in the tilt misorientation between a GB under consideration and the low-energy boundary (where θ_0 is close to θ).

During the bowing of a high-angle GB, the displacements of GB dislocations from their initial (equilibrium) positions (Fig. 7(a)) to new positions in the curved state of the GB (Fig. 7(b)) give rise to re-arrangement of the stress field created by these dislocations. This re-arrangement is also strongly affected by the misorientation balance at the junctions of GBs. As with low-angle tilt boundaries described in the previous sections, the triple junctions adjacent to the GB are assumed to be compensated. That is, the junctions A and B play the role of stress sources compensating for the stress field of a finite dislocation wall consisting of GB dislocations with Burgers vectors value b_{gb}. In these circumstances, the upper and bottom junctions A and B adjacent to the high-angle tilt boundary with GB dislocations carrying tilt $\theta-\theta_0$ are described as those containing disclinations that completely compensate for the stress field of a finite dislocation wall consisting of GB dislocations. According to formula (4), the compensating disclinations at junctions A and B are characterized by the strength values $\omega=\theta-\theta_0$ and $-(\theta-\theta_0)$, respectively.

With the above analysis of geometry of a high-angle GB and its dislocations, we describe bowing of the boundary as a process related to movement of GB dislocations under the shear stress action, using the same scheme as with movement of lattice dislocations composing a low-angle tilt boundary (see Sections 2–4). In this case, we use dislocation dynamics equations (2) with the force F_i (on the right-hand side of Eq. (2)), written in the following form:

$$F_i=\tau b_{gb}+Db_{gb}\left[b_{gb}\sum_{\substack{k=1\\k\neq i}}^{N}\frac{(x_i-x_k)\{(x_i-x_k)^2-(y_i-y_k)^2\}}{\{(x_i-x_k)^2+(y_i-y_k)^2\}^2}-\omega\left(\frac{x_iy_i}{x_i^2+y_i^2}-\frac{x_i(y_i-d)}{x_i^2+(y_i-d)^2}\right)\right]-F_i^{gb}. \tag{5}$$

Here F_i^{gb} is the hampering force that acts on the i th GB dislocation due to the bowing-induced increase in the GB length and the corresponding increase ΔW_{gb} of the GB energy. The energy increase ΔW_{gb} is given by $\Delta W_{gb}=\gamma_{gb}\Delta l_{gb}$, where γ_{gb} is the specific energy (per unit area) of the GB, and $\Delta l_{gb}=l_{gb}-d$ is the bowing-induced increase in the GB length from its initial value d to the value l_{gb} characterizing the curved state of the boundary. The curved line of the GB (Fig. 7(b)) is well approximated as that consisting of short straight segments which join neighboring GB dislocations. In this situation, the length of the curved boundary is given by the following approximate formula: $l_{gb}\approx\sum_{k=1}^{N+1}\sqrt{(x_k-x_{k-1})^2+h^2}$, where $x_0=x_{N+1}=0$. With this formula and the above formula for the GB energy increase ΔW_{gb}, we find the hampering force F_i^{gb} to be as

$$\begin{aligned}F_i^{gb}&=\frac{d(\Delta W_{gb})}{dx_i}\\&=\gamma_{gb}\frac{d}{dx_i}\left(\sum_{k=1}^{N+1}\sqrt{(x_k-x_{k-1})^2+h^2}-d\right)\\&=\gamma_{gb}\left(\frac{x_i-x_{i-1}}{\sqrt{(x_i-x_{i-1})^2+h^2}}+\frac{x_i-x_{i+1}}{\sqrt{(x_i-x_{i+1})^2+h^2}}\right).\end{aligned} \tag{6}$$

Solution of the system (2) with the force given by formulas (5) and (6) allows us to find new equilibrium positions (x_{0i},y_{0i}), $i=1,2,\ldots,N$, of GB dislocations and, as a corollary, an equilibrium configuration of the high-angle GB in its curved state (Fig. 7(b)). This configuration is characterized by the distance x_{max} between the center point of the curved boundary and the initial straight boundary line. With the solution of dislocation dynamics Eqs. (2), (5) and (6), we have calculated the dependences of x_{max} on the disclination strength ω (see Fig. 8(a)) and the GB length d (see Fig. 8(b)). As follows from Figs. 8(a) and (b), these dependences are close to linear ones.

Now let us consider the emission of partial dislocations from a curved high-angle GB under the shear stress action. For definiteness, we assume that one of the GB dislocations located at the curved boundary splits into an immobile GB dislocation and a mobile Shockley dislocation that moves in the adjacent grain interior (Fig. 7(c)). The partial Shockley dislocation is characterized by its Burgers vector with the edge component $\boldsymbol{b}_e$ and screw component $\boldsymbol{b}_s$. Its movement is accompanied by the stacking fault formation behind it (Fig. 7(c)). The stacking fault is characterized by the length l_p and the specific energy γ (per unit area of the fault). The immobile GB dislocation located at the position of the initial dislocation is characterized by its Burgers vector with the edge component $\boldsymbol{b}_{gb}-\boldsymbol{b}_e$ and screw component $-\boldsymbol{b}_s$.

In our previous consideration of bowing and decay of low-angle tilt boundaries (see Sections 2–4), we have neglected the misorientation of dislocation glide planes relative to the normal to the tilt boundary plane. It was assumed that lattice dislocations move along their glide planes which are perpendicular to the boundary plane. This assumption is correct for the case of low-angle boundaries, but not for high-angle GBs. Therefore, in our analysis of the dislocation emission from high-angle GBs (Fig. 7(c)), we consider movement of the Shockley dislocation along a glide plane misoriented by $\theta/2$ relative to the normal to the GB plane in its initial state (Fig. 7(a)). This corresponds to the case of symmetric tilt boundaries.

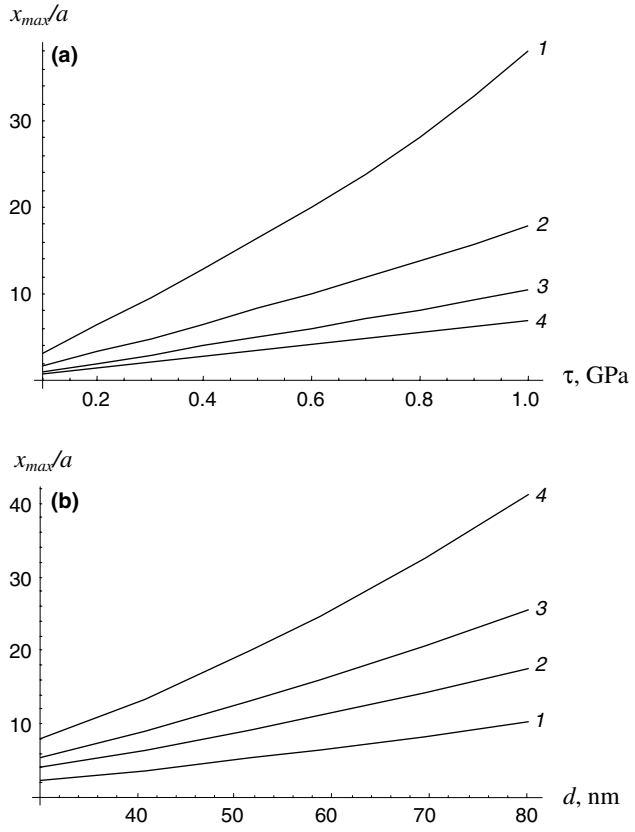

Fig. 8. Dependences of the characteristic distance $x_{\max}$ on the parameters of a deformed nanocrystalline material: (a) $x_{\max}$ via the external shear stress τ for $N = 20$ and $\omega = 4°$, 6°, 8°, and 10° (curves 1, 2, 3, and 4, respectively); (b) $x_{\max}$ via the boundary length (grain size) d for $\omega = 4°$ (with the number of dislocations N varying with d) and $\tau = 0.3$, 0.5, 0.7, and 1 GPa (curves 1, 2, 3 and 4, respectively).

Let us calculate the energy characteristics of the dislocation emission considered as a transformation of the system from its initial state (Fig. 7(b)) to the final state (Fig. 7(c)). The dislocation emission is energetically favorable, if the energy difference

$$\Delta W = W_2 - W_1 - A_\tau \tag{7}$$

is negative ($\Delta W < 0$). Here W_1 and W_2 are the energies of the defect system in its initial (Fig. 7(b)) and final (Fig. 7(c)) states, respectively, and A_τ is the work spent to transfer the Shockley dislocation under an external stress τ.

The energy W_1 consists of the four terms:

$$W_1 = W_{\rm el}^{\omega} + W_{\rm el}^{\rm gb} + W_{\rm int}^{\omega\text{–gb}} + NW_{\rm c}^{\rm gb}, \tag{8}$$

where $W_{\rm el}^{\omega}$ denotes the elastic energy of the disclination dipole, $W_{\rm el}^{\rm gb}$ the sum elastic energy of the GB dislocations, $W_{\rm int}^{\omega\text{–gb}}$ the energy of interaction between the disclination dipole and the GB dislocations, and $NW_{\rm c}^{\rm gb}$ the sum energy of the GB dislocation cores (with N being the number of dislocations located at the high-angle boundary).

In order to calculate the energy W_2 of the defect system shown in Fig. 7(c), it is convenient to represent the formation of the Shockley dislocation as that of two dislocation dipoles: a dipole of edge dislocations and a dipole of screw dislocations (Fig. 9). In the framework of this representation, the energy W_2 consists of twelve terms:

$$W_2 = W_{\rm el}^{\omega} + W_{\rm el}^{\rm gb} + W_{\rm int}^{\omega\text{–gb}} + W_{\rm el}^{\rm dip\text{–e}} + W_{\rm el}^{\rm dip\text{–s}} + W_{\rm int}^{\omega\text{–e}} + W_{\rm int}^{\rm gb\text{–e}} + (N-1)W_{\rm c}^{\rm gb} + W_{\rm c}^{\rm e} + 2W_{\rm c}^{\rm s} + W_{\rm c}^{\rm dif} + \gamma l_{\rm p}. \tag{9}$$

Here $W_{\rm el}^{\rm dip\text{–e}}$ and $W_{\rm el}^{\rm dip\text{–s}}$ are the self elastic energies of the edge and screw dislocation dipoles, respectively; $W_{\rm int}^{\omega\text{–e}}$ and $W_{\rm int}^{\rm gb\text{–e}}$ are the energies of elastic interaction of the edge dislocation dipole with the disclination dipole and the GB dislocations, respectively; $W_{\rm c}^{\rm e}$ and $W_{\rm c}^{\rm s}$ are the energies of the edge and screw components of the Shokley dislocation cores, respectively; $W_{\rm c}^{\rm dif}$ the core energy of the immobile (difference) GB dislocation resulted from the splitting of the initial GB dislocation.

With formulas (7)–(9), the characteristic energy difference ΔW can be written as follows:

$$\Delta W = W_{\rm el}^{\rm dip\text{–e}} + W_{\rm el}^{\rm dip\text{–s}} + W_{\rm int}^{\omega\text{–e}} + W_{\rm int}^{\rm gb\text{–e}} - W_{\rm c}^{\rm gb} + W_{\rm c}^{\rm e} + 2W_{\rm c}^{\rm s} + W_{\rm c}^{\rm dif} + \gamma l_{\rm p} - A_\tau. \tag{10}$$

The self energies and the interaction energies figuring on the right-hand side of formula (10) are calculated in a standard way as the works spent to generate the defects in the stress fields created by the same and other defects, respectively; see, e.g., [20,44]. The defect core energies are given by standard approximate formulas which may be found in [40]. The work A_τ is given by $A_\tau = \tau_{x'y'} b_{\rm e} l_{\rm p}$, where $\tau_{x'y'}$ is the component of the external shear stress tensor written in the $Ox'y'$ coordinate system (Fig. 9). After some algebra operating with the above standard formulas, we find the following expression for ΔW:

$$\Delta W = \frac{D}{2}\left[b_{\rm e}^2\left(2\ln\frac{l_p - b_{\rm e}}{b_{\rm e}} + 1\right) + 2(1-\nu)b_{\rm s}^2\left(\ln\frac{l_p - b_{\rm s}}{b_{\rm s}} + 1\right) - b_{\rm gb}^2 + b_{\rm dif}^2\right] + b_{\rm e}\int_{b_e}^{l_p}\left[\sigma_{x'y'}^{\omega}(x', y' = 0) + \sigma_{x'y'}^{\rm gb}(x', y' = 0)\right]dx' + l_{\rm p}(\gamma - \tau_{x'y'}b_{\rm e}). \tag{11}$$

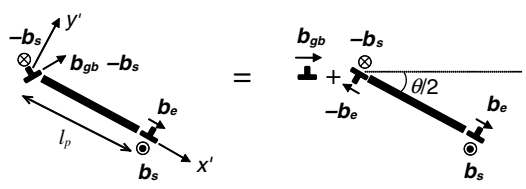

Fig. 9. Split dislocation configuration, consisting of a leading partial Shockley dislocation and a difference dislocation, is represented through the pre-existent grain boundary dislocation and two dislocation dipoles composed of edge and screw dislocations.

Here $b_{\mathrm{dif}} = \sqrt{(b_{\mathrm{gb}} - b_{\mathrm{e}}\cos\theta/2)^2 + b_{\mathrm{e}}^2 \sin^2\theta/2}$ is the Burgers vector magnitude that characterizes the immobile (difference) GB dislocation resulted from the splitting of the pre-existent GB dislocation (Fig. 9); $\sigma^{\omega}_{x'y'}$ and $\sigma^{\mathrm{gb}}_{x'y'}$ are the components of the stress tensors of the disclination dipole and the GB dislocation wall, respectively. The components are written in the coordinate system $Ox'y'$ associated with the pre-existent GB dislocation (Fig. 9). Transformation of the stress tensor components written in the coordinate system Oxy (Fig. 7) into those written in the coordinate system $Ox'y'$ (Fig. 9) is described in the standard way as follows:

$$\sigma_{x'y'}(x',y') = \sigma_{xy}(x,y)\cos\theta - \frac{\sin\theta}{2}[\sigma_{yy}(x,y) - \sigma_{xx}(x,y)], \tag{12}$$

where $x = x'\cos\theta/2 - y'\sin\theta/2 + x_d$ and $y = -x'\sin\theta/2 + y'\cos\theta/2 + y_d$. Here x_d and y_d are the coordinates of the pre-existent GB dislocation; they are defined using a description of the bowing of the high-angle boundary (see an analysis in the first part of this section). In formula (11), the core radii of dislocations are assumed to be equal to the Burgers vector magnitudes of these dislocations. Calculation of the integral figuring on the right-hand side of formula (11) is a routine elementary procedure. It results in a very space-consuming expression which therefore is not presented here.

With formula (11), we have calculated the characteristic energy difference ΔW in the exemplary case of pure nanocrystalline Cu. In doing so, we have used the following characteristic values of parameters: $G = 48$ GPa, $\nu = 0.34$, the crystal lattice parameter $a = 3.6$ Å, the typical Burgers vector $\frac{a}{2}\langle 110\rangle$ having the magnitude $b = 2.55$ Å, $\rho = 8920$ kg m^{-3}, $m = 2.9 \times 10^{-16}$ kg m^{-1}, $\beta = 5 \times 10^{-5}$ Pa s, $\gamma = 0.06$ J m^{-2}. The Burgers vector magnitude characterizing an elementary mobile GB dislocation is assumed to be $b_{\mathrm{gb}} = b/2$. The screw and edge components of the Burgers vector for a Shockley dislocation are $b_{\mathrm{s}} = a/(2\sqrt{6})$ and $b_{\mathrm{e}} = b/2$, respectively. The specific energy γ_{gb} of a high-angle boundary depends on the tilt misorientation θ_0 of a low-energy boundary. Following [45], the $\Sigma = 5/(210)$ with $\theta_0 = 36.87°$ in Cu is characterized by the specific energy $\gamma_{\mathrm{gb}} = 0.9$ J m^{-2}. Generally speaking, values of γ_{gb} in Cu vary in the range from 0.7 to 1 J m^{-2}.

A typical curve $\Delta W(l_{\mathrm{p}})$ is shown in Fig. 10(a). It has been calculated for the case when a high-angle boundary contains 20 GB dislocations, for $\tau = 1$ GPa, $\omega = 3°$ and the above values of other parameters. It may seem that the taken value 1 GPa for τ is too high for Cu. However, it has recently been shown by atomic scale simulations [21,46] that this local stress level is real for nanocrystalline Cu with grain size ranging from roughly 5 to 50 nm. In this case, τ is treated as the *local* stress acting in the area under consideration. Fig. 10(a) characterizes the splitting of the 5th GB dislocation numerated from the lower GB junction; it is the most favorable splitting process compared to those of other GB dislocations.

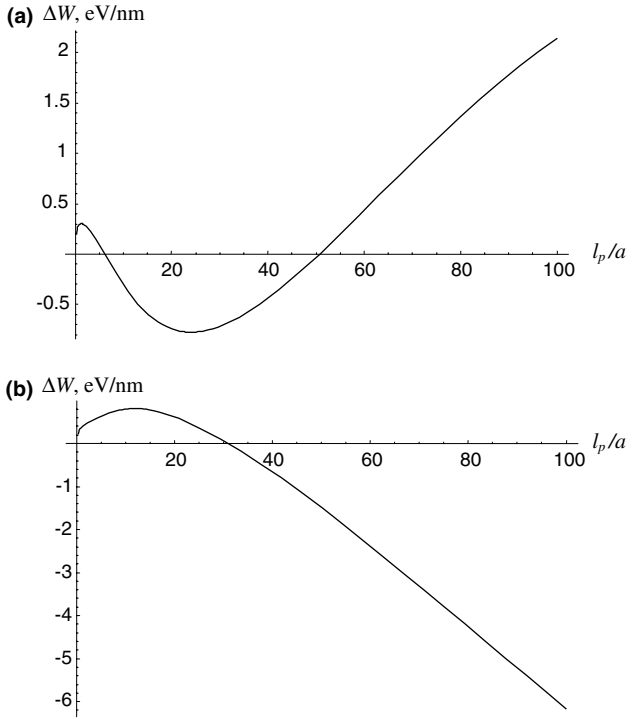

Fig. 10. Typical dependences of the characteristic energy change ΔW on the path l_{p} moved by a partial Shockley dislocation in the case of high-angle boundary containing $N = 20$ grain boundary dislocations, for $\tau = 1$ GPa and $\omega = 3°$: (a) splitting of the 5th grain boundary dislocation, and (b) splitting of the 1st grain boundary dislocation.

As follows from Fig. 10(a), an energetic barrier exists at the beginning of the curve $\Delta W(l_{\mathrm{p}})$, which hinders the GB dislocation splitting. Two terms contribute to the energetic barrier: a term related to the elastic interaction between the dislocations and disclinations, and a term describing dramatic change in the dislocation core energy due to the splitting. The interaction energy contribution to the barrier is relatively low; its typical values are in the range from 0.01 to 0.2 eV/nm. In addition, its maximum corresponds to the distance $l_{\mathrm{p}} \approx (1-2)a$ between the immobile and mobile partial dislocations. The classic linear elasticity approach used in our calculation of the interaction energy is too approximate at this length scale. In these circumstances, it is senseless to make a more detailed analysis of relationship between the energetic barrier height and the parameters of the system under consideration. With results of our analysis, we can just conclude that the interaction energy causes a small contribution ($\leqslant 0.2$ eV/nm) to the energetic barrier for partial dislocation movement in vicinity of the immobile GB dislocation. The second (core) contribution is characterized by a typical value about 0.2 eV/nm and does not depend on l_{p} and other parameters.

To summarize, there is an energetic barrier for the splitting of GB dislocations in high-angle boundaries under the shear stress action. Its height is about 0.2–0.4 eV/nm. With the closest interatomic distance ≈0.25 nm, we find that the energy barrier per one atom is about 0.05–0.1 eV. This value is close to the characteristic energy ≈0.025 eV of thermal fluctuations at room temperature. In these circumstances, the energetic barrier can be easily overcome by GB dislocations.

The dependence $\Delta W(l_p)$ shown in Fig. 10(a) has also a minimum that causes the equilibrium distance between the partial dislocations resulted from the splitting. In the case illustrated in Fig. 10(a), the equilibrium distance is about $23a$. Notice, however, that a minimum is inherent to the dependence $\Delta W(l_p)$ in only certain ranges of parameters of the system, but not always. For illustration, let us consider the dependence $\Delta W(l_p)$ in Fig. 10(b) which characterizes the splitting of the 1st dislocation and is calculated for the same values of parameters as the dependence shown in Fig. 10(a). The energetic barrier for the splitting of the 1st dislocation—a maximum magnitude of the curve shown in Fig. 10(b)—is larger that that characterizing the splitting of the 5th dislocation (Fig. 10(a)). In this case, the splitting of the 1st dislocation is less probable compared to the splitting of the 5th dislocation. At the same time, there is no minimum of the dependence $\Delta W(l_p)$ in Fig. 10(b). This means that the equilibrium splitting distance is absent, and the partial dislocation resulted from the splitting of the 1st dislocation moves in the adjacent grain interior until it reaches some structural obstacle (e.g., another GB) for its movement.

Now let us examine sensitivity of the dependence $\Delta W(l_p)$ to the external shear stress τ. The curves $\Delta W(l_p)$ are presented in Fig. 11(a) for $\gamma_{gb} = 0.9$ J m^{-2}, $\omega = 3°$, $N = 20$ and different values of the external shear stress $\tau = 0.4$, 0.6, 0.8 and 1 GPa. As follows from Fig. 11(a), an increase in τ enhances the splitting of a GB dislocation, followed by emission of a Shockley dislocation into the grain interior. At the same time, the dislocation emission is energetically unfavorable at low values of τ.

The dependence $\Delta W(l_p)$ is also very sensitive to the value of the disclination strength ω. The curves $\Delta W(l_p)$ are shown in Fig. 11(b) for $\tau = 1$ GPa, $N = 20$, $\gamma_{gb} = 0.9$ J m^{-2} and different values of $\omega = 3°$, 5°, 7° and 9°. As follows from Fig. 11(b), the dislocation emission from high-angle boundary is hampered with rising ω.

It is worth noting that our model is applicable at relatively small τ and large ω. For higher stresses ($\tau >$ 1 GPa) and lower disclination strengths ($\omega < 3°$), our model high-angle boundary decays which means that the model becomes incorrect.

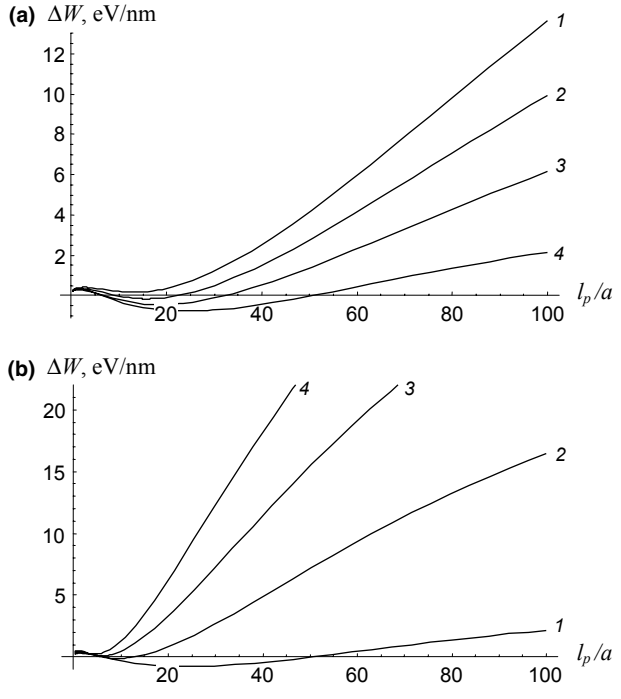

Fig. 11. Dependences of the characteristic energy change ΔW on the path l_p moved by the 5th partial Shockley dislocation in the case of high-angle boundary containing $N = 20$ grain boundary dislocations, for (a) $\omega = 3°$ and different values of the external shear stress $\tau = 0.4$, 0.6, 0.8, and 1.0 GPa (curves 1, 2, 3 and 4, respectively); and (b) $\tau = 1$ GPa and different values of the disclination strength $\omega = 3°$, 5°, 7°, and 9° (curves 1, 2, 3 and 4, respectively).

6. Conclusions

In this paper, we have theoretically described transformations of GBs in deformed NCMs. In particular, it has been shown that the decay of a low-angle tilt boundary in a mechanically loaded nanocrystalline solid gives rise to local plastic deformation in the grain where the low-angle boundary decay has occurred and in its neighbouring grains. Lattice dislocations released from the decayed low-angle boundary enhance decay of neighboring low-angle tilt boundaries (Fig. 4). Also, decay of a low-angle tilt boundary leads to the formation of a dipole of disclinations at the grain boundary junctions adjacent to the decayed boundary (Figs. 1(d), 4 and 5). The disclination dipole elastically interacts with the lattice dislocations composing neighboring low-angle tilt boundaries and enhances decay of these boundaries (Fig. 5). Thus, the shear-stress-induced decay of a low-angle tilt boundary can trigger the formation of a shear band (thin, sheet-like region where high plastic strain is localized) in the nanocrystalline solid. In this event, the critical shear stress τ_c characterizes the initial stage of local plastic deformation occurring via generation and development of shear bands. According to our calculations (see Fig. 3), the shear stress τ_c ranges from 0.5 GPa (for $\theta \approx 2°$) to 2.5 GPa (for $\theta \approx 10°$), that characterizes the decay of low-angle tilt boundaries with different misorientation parameters in nanocrystalline

Fe. Its mean value $\langle \tau_c \rangle = 1.5$ GPa coincides with the experimentally measured [39] value of the shear stress at which shear bands with elongated grain structure are formed in nanocrystalline Fe. It is worth noting that a similar process of decay of a low-angle boundary has recently been observed in molecular dynamics simulations [47] of plastic deformation in nanocrystalline Ni.

Also, in this paper, we have theoretically examined the bowing of high-angle GBs and emission of partial dislocations from such boundaries under the shear stress action (Fig. 7). Both these transformations are found to be highly sensitive to the shear stress τ that acts on a high-angle grain boundary and the parameter ω characterizing the density of GB dislocations at the boundary (Fig. 11). The results of our theoretical model account for experimental observations of curved GBs [1,33] and emission of partial dislocations by GBs [32–35] in deformed nanocrystalline metals. The latter has also been observed in molecular dynamics simulations of plasticity processes in nanocrystalline Al [23,24], Cu [21,22,46–50] and Ni [22,47–52].

Our results are indicative of the important role of the behavior of intrinsic GB dislocations in the transformations of high-angle boundaries. In NCMs, where GBs serve as effective obstacles for movement of lattice dislocations, and the action of lattice dislocation sources in grain interiors is suppressed, the external stress level is high enough to drive movement and/or splitting of intrinsic GB dislocations at high-angle GBs. As a result, high-angle boundaries undergo the specific transformations which are capable of essentially modifying the actions of deformation and fracture mechanisms (highly sensitive to GB structural geometry [19,20,53]) in NCMs.

Acknowledgements

This work was supported, in part, by the Office of US Naval Research (Grant N00014-01-1-1020), INTAS (Grant 03-51-3779), Russian State Research Program on Solid-State Nanostructures, Russian Science Support Foundation, the Russian Fund of Basic Research (Grant 04-01-00211), Russian Academy of Sciences Program "Structural Mechanics of Materials and Constructions", St. Petersburg Scientific Center, and "Integration" Program (Grant B0026).

References

[1] Kumar KS, Suresh S, Chisholm MF, Horton JA, Wang P. Acta Mater 2003;51:387.
[2] Jia D, Ramesh KT, Ma E. Acta Mater 2003;51:3495.
[3] Schwaiger R, Moser B, Dao M, Chollacoop N, Suresh S. Acta Mater 2003;51:5159.
[4] Kumar KS, Swygenhoven H, Suresh S. Acta Mater 2003;51:5743.
[5] Valiev RZ, Sergueeva AV, Mukherjee AK. Scr Mater 2003;49:669.
[6] Mukherjee AK. Mater Sci Eng A 2002;322:1.
[7] Zhan G-D, Kuntz JD, Wan J, Mukherjee AK. In: Berndt CC, Fischer T, Ovid'ko IA, Skandan G, Tsakalakos T, editors. Nanomaterials for structural applications. MRS Symposium Proceedings, vol. 740. Warrendale: MRS; 2003. p. 41.
[8] Wei Q, Jia D, Ramesh KT, Ma E. Appl Phys Lett 2002;81:1240.
[9] Koch CC. Rev Adv Mater Sci 2003;5:91.
[10] Murayama M, Howe JM, Hidaka H, Takaki S. Science 2002;295:2433.
[11] Hahn H, Padmanabhan KA. Philos Mag B 1997;76:559.
[12] Masumura RA, Hazzledine PM, Pande CS. Acta Mater 1998;46:4527.
[13] Konstantinidis DA, Aifantis EC. Nanostruct Mater 1998;10:1111.
[14] Ovid'ko IA. Science 2002;295:2386.
[15] Fedorov AA, Gutkin MYu, Ovid'ko IA. Acta Mater 2003;51:887.
[16] Gutkin MYu, Ovid'ko IA, Skiba NV. Acta Mater 2003;51:4059.
[17] Cheng S, Spencer JA, Milligan WW. Acta Mater 2003;51:4505.
[18] Bobylev SV, Gutkin MYu, Ovid'ko IA. J Phys D 2004;37:269.
[19] Ovid'ko IA, Sheinerman AG. Acta Mater 2004;52:1201.
[20] Gutkin MYu, Ovid'ko IA. Plastic deformation in nanocrystalline materials. Berlin: Springer; 2004.
[21] Schiotz J, Vegge T, Di Tolla FD, Jacobsen KW. Phys Rev B 1999;60:11971.
[22] van Swygenhoven H, Spaczer M, Caro A, Farkas D. Phys Rev B 1999;60:22.
[23] Yamakov V, Wolf D, Phillpot SR, Mukherjee AK, Gleiter H. Nat Mater 2002;1:45.
[24] Yamakov V, Wolf D, Phillpot SR, Mukherjee AK, Gleiter H. Acta Mater 2002;50:5005.
[25] Sutton AP, Balluffi RW. Interfaces in crystalline materials. Oxford: Oxford Science Publications; 1996.
[26] Ankem S, Pande CS, Ovid'ko IA, Ranganathan S, editors. Interface science and technology TMS Symposium Proceedings. Warrendale: TMS; 2002.
[27] Gutkin MYu, Ovid'ko IA. Phys Rev B 2001;63:064515.
[28] Bobylev SV, Ovid'ko IA. Phys Rev B 2003;67:132506.
[29] Ruano OA, Wadsworth J, Sherby OD. Acta Mater 2003;51:3617.
[30] Koch CC. Scr Mater 2003;49:657.
[31] Ma E. Scr Mater 2003;49:663.
[32] Chen MW, Ma E, Hemker KJ, Sheng HW, Wang YM, Cheng XM. Science 2003;300:1275.
[33] Liao XZ, Zhou F, Lavernia EJ, Srinivasan SG, Baskes MI, He DW, et al. Appl Phys Lett 2003;83:632.
[34] Liao XZ, Zhou F, Lavernia EJ, He DW, Zhu YT. Appl Phys Lett 2003;83:5062.
[35] Liao XZ, Zhou F, Srinivasan SG, Zhu YT, Valiev RZ, Gunderov DV. Appl Phys Lett 2004;84:592.
[36] Gutkin MYu, Kolesnikova AL, Ovid'ko IA, Skiba NV. Philos Mag Lett 2002;81:651.
[37] Gutkin MYu, Ovid'ko IA, Skiba NV. Mater Sci Eng A 2003;339:73.
[38] Zghal S, Hytch SJ, Chevalier J-P, Twesten R, Wu P, Bellon P. Acta Mater 2002;50:4695.
[39] Wei Q, Jia D, Ramesh KT, Ma E. Appl Phys Lett 2002;81:1240.
[40] Hirth JP, Lothe J. Theory of Dislocations. New York: Wiley; 1982.
[41] Romanov AE, Vladimirov VI. In: Nabarro FRN, editor. Dislocations in solids, vol. 9. Amsterdam: North Holland; 1992. p. 191.
[42] Kocks UF, Argon AS, Ashby MF. Prog Mater Sci 1975;19:1.
[43] Weertman JR, Sanders PG. Solid State Phenom 1994;35–36:249.
[44] Mura T. Micromechanics of defects in solids. Dordrecht: Martinus Nijhoff; 1987.
[45] Udler D, Seidman DN. Phys Rev B 1996;54:R11133.
[46] Schiotz J, Jacobsen KW. Science 2003;301:1357.
[47] Hasnaoui A, van Swygenhoven H, Derlet PM. Phys Rev B 2002;66:184112.
[48] van Swygenhoven H, Spaczer M, Caro A. Acta Mater 1999;47:3117.

[49] Derlet PM, van Swygenhoven H. Scr Mater 2002;47:719.
[50] Derlet PM, Hasnaoui A, van Swygenhoven H. Scr Mater 2003;49:629.
[51] van Swygenhoven H, Derlet PM, Hasnaoui A. Phys Rev B 2002;66:024101.
[52] Swygenhoven H, Derlet PM, Hasnaoui A, Samaras M. In: Tsakalakos T, Ovid'ko IA, Vasudevan AK, editors. Nanostructures: synthesis, functional properties and applications. Dordrecht: Kluwer; 2003. p. 155.
[53] Gutkin MYu, Ovid'ko IA, Skiba NV. Acta Mater 2004;52:1711.